# Numerical and Mechanical Research on Withdrawal Capacity of Parallel-to-grain Connection Part of Mortise and Loose Tenon Joint for Wooden Furniture

Jie Chen, and Huiyuan Guan *

The mortise and loose tenon (M&LT) joint is a form between mortise-and-tenon (M&T) joint and dowel. It combines the advantages of easy processing and high bonding strength and has no requirement for the shape of the tenon shoulder. However, there is a lack of research conducted separately on the parallel-to-grain part of M&LT joint. This study explored the withdrawal capacity of the equivalence I-type specimen to focus on the strength of the parallel-to-grain part of M&LT joint by conducting mechanical experiments and establishing finite element model. The results indicated that (1) The largest average pull-out load occurred at the group of 0.1 mm interference fit with the value of 16000 N, most of the joints underwent shear damage of material parallel-to-grain; (2) The maximum load of FEM is 14300 N with an error of 10.5%, so finite element model is a rational approach to predict the withdrawal strength of parallel-to-grain connection of M&LT joint.

*Contact information: Department of Furniture Design, Nanjing Forestry University, 210037 Nanjing, China;*Corresponding author: guanhuiyuan@njfu.com.cn*

## INTRODUCTION

The oval mortise-and-tenon (M&T) joint is commonly used in modern wood furniture frames (Bayatkashkoli *et al.* 2017). Many studies have found various factors that affect the tensile capacity and bending moment capacity of M&T joints, by carrying out mechanical experiments, or using Finite Element Method (Xie *et al.* 2021) and Analytic Method (AM) (Smardzewski 2002). A lot of research focused on the macroscopic conditions of joints by carrying out basic mechanical experiments. Some scholars have studied the effects of type of loading, wood species, geometric parameters of tenon (Oktaee *et al.* 2014; Vassilios *et al.* 2016), type of adhesive (Kasal *et al.* 2013), and connection methods (Miao *et al.* 2022) on tensile capacity (Derikvand *et al.* 2013; Diler *et al.* 2017), bending moment capacity and stiffness, and fatigue strength (Ratnasingam and Ioras 2013). In general, it has been found that these influencing factors all have a significant impact on the various strengths of M&T joints. Subsequently, the finite element method (FEM) was also applied to simulate the strength of furniture joints. Hu (2020, 2021) and Fu (2022) combined finite element analysis (FEA) with response surface method (RSM) to investigate the effect of tenon geometric dimensions (length, width, and thickness) on withdrawal and bending load capacities and stiffness of mortise-and-tenon (M-T) joints. Theoretical estimation of the mechanical performance of traditional mortise-and-tenon

joint (Ogawa *et al.* 2016) is also very commonly used. The two methods have been confirmed to be rational and to stimulate the connection characteristics of M&T joints. Xu *et al.* (2023) applied a parametric optimized method of three-dimensional corner joints in wooden furniture and refined the theoretical value range of at least four main parameters. On this basis, many scholars have conducted research on connection mechanisms (Ramon *et al.* 2020) of joints. Hu *et al.* (2018; 2019) proposed a method to measure the contact forces (Jung *et al.* 2006a,b,c) and deformations of mortise and tenon joints. These researchers studied the relaxation behavior of joints for 3 h with tenons in different grain orientations and tenon fits. Based on this, Fu *et al.* (2020, 2022) studied the impact of moisture content, interference fit, and grain direction on the contact force by conducting experimental testing, establishing finite element model and theoretical model. Chen and Guan (2023) utilized this method to determine the optimal interference fit of different materials. Meanwhile, many scholars promoted the accuracy of finite element model. Igor Džinčić *et al.* (2012) considered that the type of strain, which is affected by the interference fit has impact on the changes in the Young's modulus of elasticity, and defined rate of deformation of oval M&T joint as a result of fitting influence. Fu *et al.* (2021) explored the influence of various size of contact area, direction of grain pressure, and moisture content, wood section on the frictional properties of wood surfaces, respectively. For glue application joints, the thickness and distribution of the adhesive layer (Hu and Guan 2019) were found to have an important impact on joint strength and the definition method of adhesive layer in finite element model.

From the perspective of material utilization and processing efficiency, M&LT joints are superior to M&T joints (Gao *et al.* 2019; Yue *et al.* 2024), and they have a wider range of applications. As shown in Fig. 1(a), the machining surface, *i.e.*, tenon shoulder, can only be machined as a plane; when using a keyway milling cutter for tenon machining, the machining surface is perpendicular to the tool. When the contact surface of frame component is required to be in the form of a curve, the M&T joint cannot meet the machining requirements. In this case, a mortise and loose-tenon (M&LT) joint can be used as a substitute. The typical M&LT joint is composed of three parts, mortise A, mortise B and tenon, the brief machining flow of these three parts shown in Fig. 1(b) indicates that there is no requirement for the shape of the shoulder in mortise machining. M&LT joint is a form between M&T joint and dowel connection (SjöDin *et al.* 2008; Hao *et al.* 2020), it has higher bonding strength than dowel connection, and compared to M&T joints, it has a more convenient machining process, is more conducive to modular design of wood furniture, as well as more in line with the concept of modern industrial production (Gao *et al.* 2019; Yue *et al.* 2024). Mohammad (Derikvand *et al.* 2013, 2014) and Hasan (Imirzi *et al.* 2015) studied the effect of geometric parameters of loose tenon on the bending moment capacity (BMC) of T-shaped and L-shaped joints, different types of joints required different geometric parameters of loose tenon, and the BMC of L-shaped joints was less than T-shaped joints.

In summary, the previous research studied the overall structure of M&LT joint but without considering the complex mechanical behavior of two parts: parallel-to-grain connection and perpendicular-to-grain connection. As shown in Fig. 1(b), the strength of M&LT joint is provided by two parts: One is the connection perpendicular to the grain between tenon and mortise A, which is similar to the M&T joint, so the strength of this part can refer to existing research on M&T joints directly. The other is the connection parallel to the grain between tenon and mortise B, but there has been little research carried out on characteristics of this part of M&LT joint separately. Empirical judgment is usually

adopted in practical use, and this may make it difficult to achieve higher strength scientifically. This study explored the mechanical behavior and withdrawal capacity of tensile strength of the parallel-to-grain connection of M&LT joint through mechanical experiments and Finite Element Method (FEM). This data will be beneficial for promoting the application of M&LT joints in practice furniture manufacturing and the industrialization of furniture production and provides more possibilities for furniture styling and modular design.
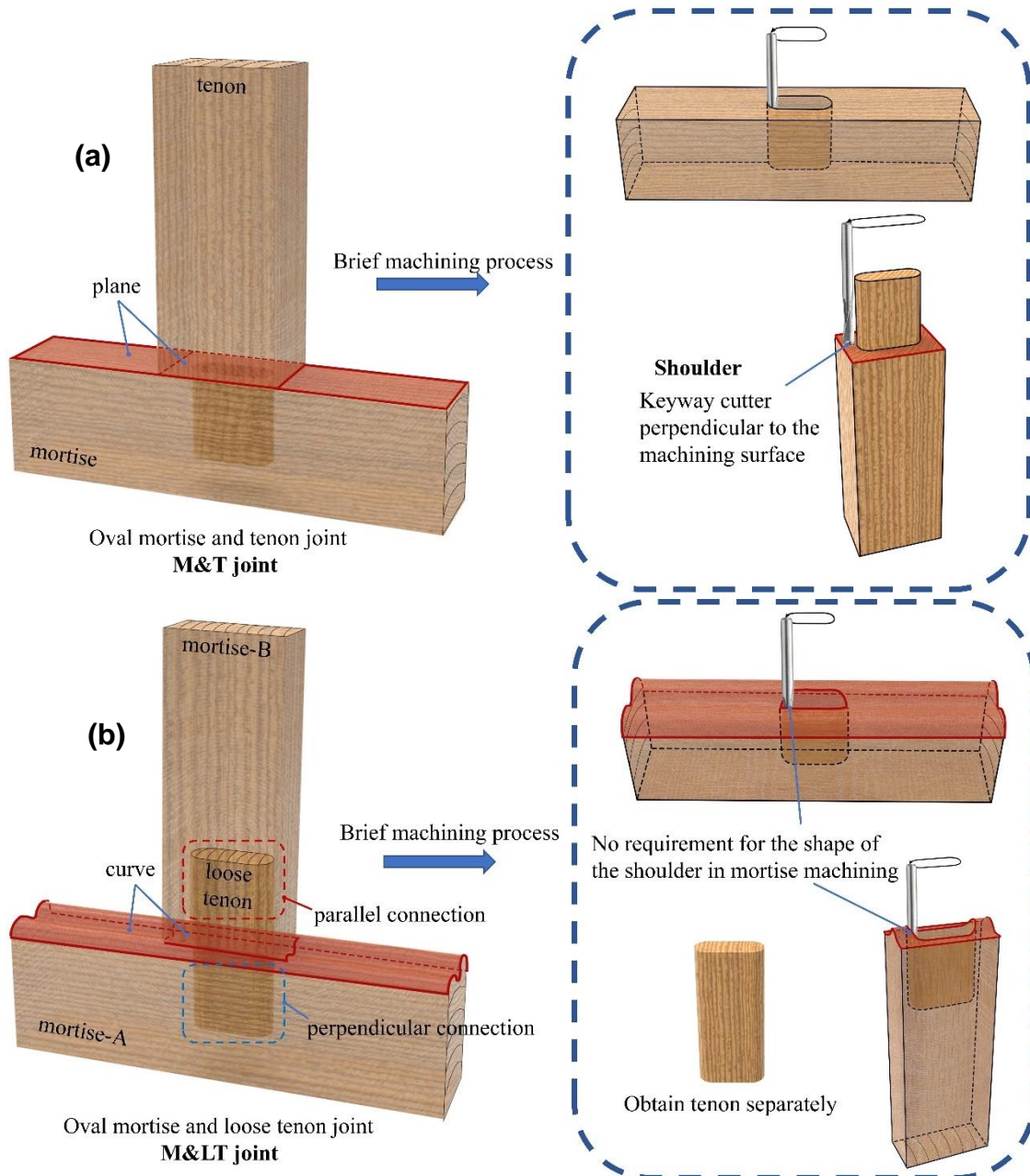


**Fig. 1.** Difference of machining process between M&T joint and M&LT joint. (a) Brief machining process of M&T joint of plane shoulder; (b) Brief machining process of M&LT joint has no requirement for the shape of shoulder.

## EXPERIMENTAL

### Materials

Beech wood (*Fagus orientalis* Lipsky) with the dimensions of 2700×180×55 mm (length × width × thickness) was purchased from a local commercial supplier (Nanjing, China). After storing in air-dried condition for 4 weeks, the moisture content of material averaged 11.7%, and the air-drying density was 0.67 g/cm$^3$.

Table 1 shows elastic constants required in finite element analysis when accounting for the basic mechanical properties of beech wood, which have been tested in previous studies (Fu *et al.* 2021), including elastic moduli, Poisson's ratios, and shear moduli (Dong *et al.* 2017).

**Table 1.** Basic Elastic Constants of Beech Wood

| Elastic Modulus (MPa) | | | Poisson's Ratio | | | | | | Shear Modulus (MPA) | | |
|---|---|---|---|---|---|---|---|---|---|---|---|
| $E_l$ | $E_R$ | $E_T$ | $U_{LR}$ | $U_{LT}$ | $U_{RT}$ | $U_{RL}$ | $U_{TR}$ | $U_{TL}$ | $G_{LR}$ | $G_{LR}$ | $G_{LR}$ |
| *13580.50* | *1747.33* | *743.96* | 0.5356 | 0.6158 | 0.8727 | 0.0618 | 0.470 | 0.029 | 843.76 | 787.30 | 199.90 |

### Configurations of Specimens

For easy machining and clamping, Fig. 2 shows an equivalent specimen of the parallel connection of M&LT joint to observe the mechanical behavior and failure mode of this part under withdrawal load separately (Lokaj *et al.* 2020).
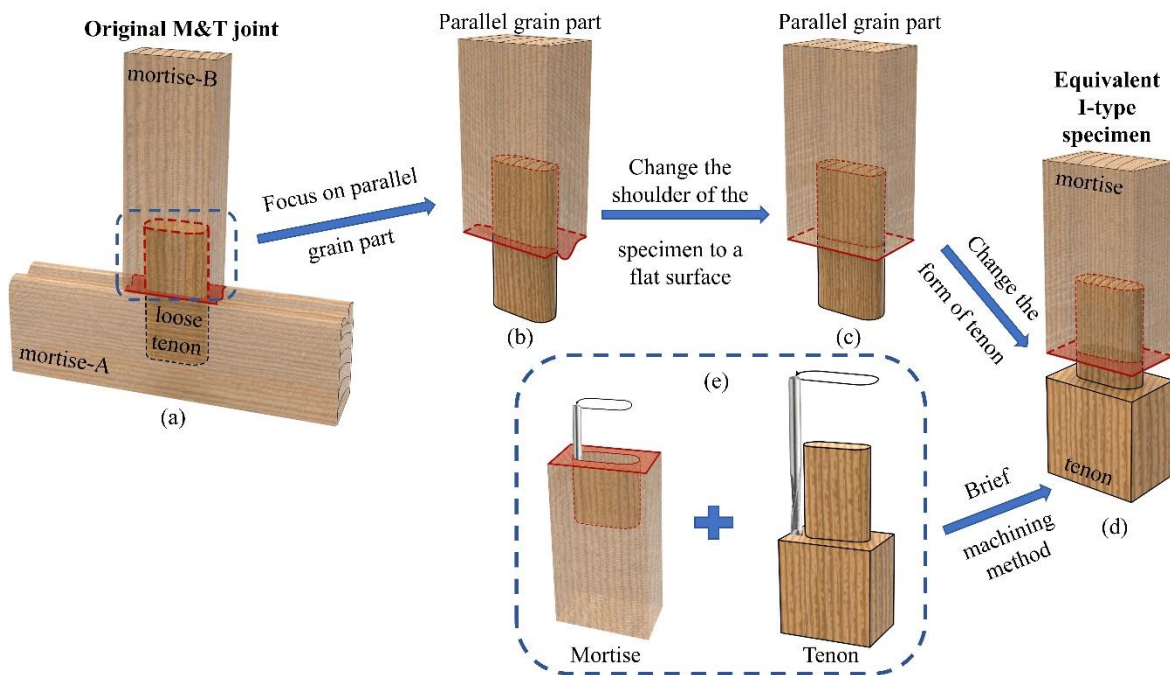


**Fig. 2.** Evolution diagram of I-type joint from oval mortise and loose tenon joint. (a) Composition of M&T joint; (b) Parallel grain part with curve shoulder; (c) Parallel grain part with plane shoulder; (d) Equivalent I-type specimen; (e) Brief machining method of I-type joint

Figure 2(a) is the original T-shaped M&LT joint. In order to focus on the joint part parallel to the grain, that is, the connection between mortise B and loose tenon member, the mortise A connected with loose tenon by perpendicular grain was removed to form the

**bioresources.cnr.ncsu.edu**

structure of Fig. 2(b). Because the shape of shoulder type has little difference to the withdrawal strength of this part (Diler *et al.* 2017; Hu *et al.* 2020), as well as to simplify the machining flow, the tenon shoulder is changed back to the plane when making the specimen to form the structure of Fig. 2(c). The form of the loose tenon that it is not sawed off from the coarse material was changed to reduce one step of machining and make it convenient to clamp the specimen for the later pull-out test, so the part of parallel-to-grain connection of original T-shaped M&LT joint was eventually evolved into the equivalent I-type specimen as shown in Fig. 2(d), and the brief machining process chart of this specimen is shown in Fig. 2(e). This alteration does not correspond to the real practical form, but a test specimen created to simplify processing steps and facilitate clamping in pull-out test.

The composition of specimen and specific dimension diagram are shown in Fig. 3. The mortise with the dimensions of 30 mm × 28 mm × 12 mm (depth × length × width) and the matched tenon with the dimensions of 40 mm × (28+$a$) mm × (12+$a$) mm (length ×width ×thickness) were milled on the prepared wood components. The fits of the direction of tenon width and thickness were set to "$a$". When "$a$" was positive, it represented an interference fit between the tenon and mortise, and when "$a$" was negative, it represented a clearance fit between the two components. The tenon length was set to be 10 mm larger than the mortise depth to ensure the two shoulders do not come into contact, prevent the adhesion of two components caused by the overflow of PVAc (White LaTeX) adhesive during assembly, which may affect the results of pull-out test. Due to the limitation of the range of auxiliary fixture, a thickness of 2.5 mm milling was applied to both sides of the clamped surfaces of tenon. All specimens were processed on a computer-numerical-control-based machine (WPC, ULI, Shanghai, China) with an accuracy of 0.01 mm.
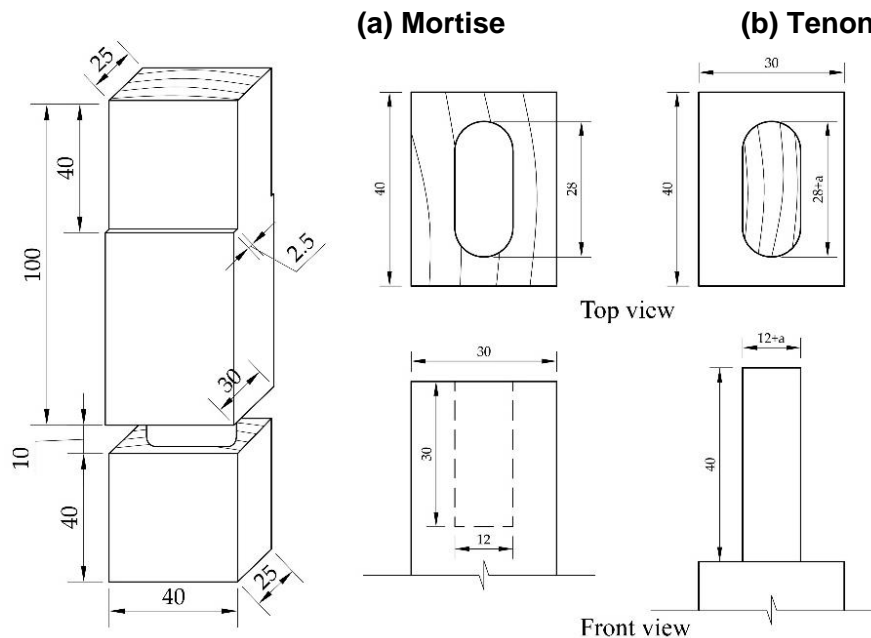


**Fig. 3.** Dimensions of I-type specimen composed of mortise (a) and tenon (b). (Unit: mm)

## Mechanical Testing

When assembling I-type joints, it is necessary to consider whether the mortise will crack. So, a preliminary experiment was conducted to indicate that if the interference fit overweighs 0.1 mm, the joint will tend to crack. Because of the limitation of interference

fit, it is speculated that the tensile strength of I-type joint is more affected by the adhesive layer. Therefore, the value of fit between mortise and tenon ranged from -0.3 mm to 0.1 mm, with an increase step of 0.1 mm, for observing the influence of fit on the formation of adhesive layer. Then, 5 groups of specimens were conducted, and each group had 30 duplicate samples, resulting in a total of 150 I-type specimens. All mortises and tenons were coated with PVAc at a rate of 150 to 220 $g/m^2$. After assembly, all specimens were placed in a constant temperature oven at 22 ℃ for 7 days for curing adhesive. The diagram of clamping specimen and tensile loading method is shown in Fig. 4. A digital vernier caliper of hundred-millimeter accuracy was used to check the dimensions of the specimen. A universal testing machine (AGS-X, SHIMADZU, Japan) was used to measure the withdrawal behavior of testing joints.
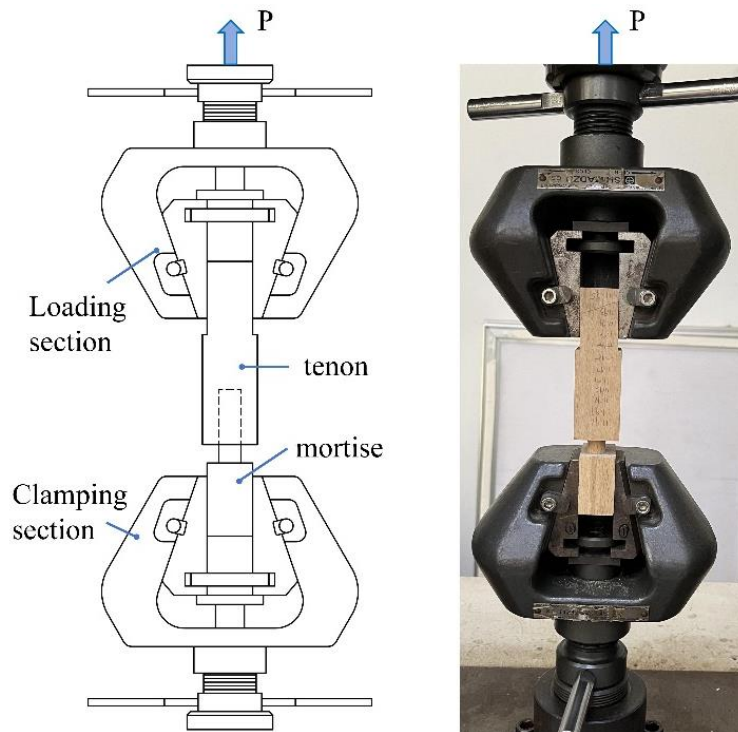


**Fig. 4.** Loading and clamping diagrams of I-type joint
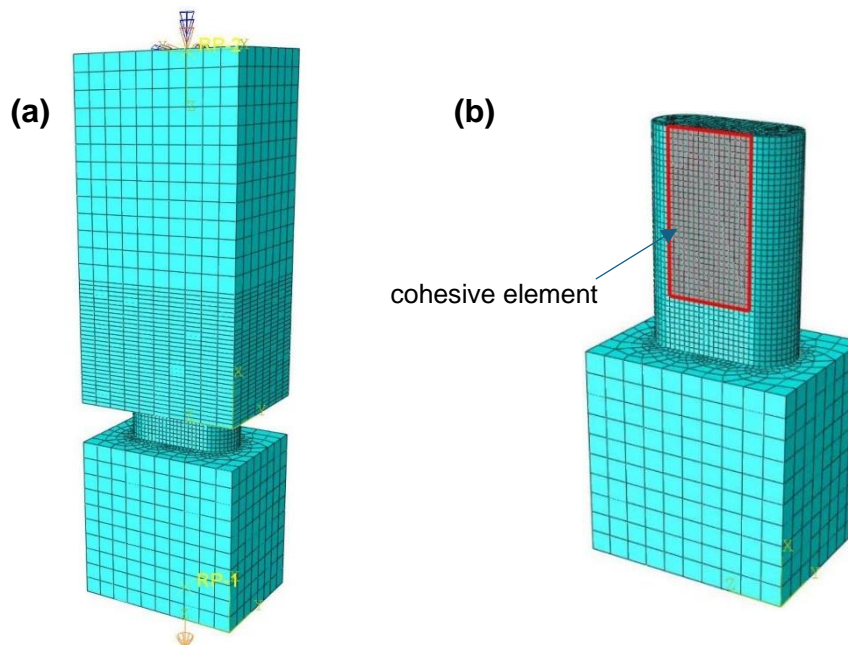
### Finite Element Model

The finite element model provides a low-cost method for simulating the tensile strength of M&LT joints parallel to the grain. Based on mechanical experimental results, the group of joints with the highest tensile strength was simulated. The output of stress and strain cloud maps and load-displacement curves was compared with the actual experimental results to analyze similarities and differences and verify the rationality of the model.

The specific modeling process is shown in Table 2. It is worth noting that the contact method (clearance fit or interference fit) and friction coefficient were defined in the arc section of the contact surface. The cohesive element was inserted between the flat part, and the thickness of adhesive layer referred to Hu's research conclusion (Hu *et al*. 2019). And the model is shown in Fig. 5.

**Table 2.** Specific Modeling Process of FEM Analysis

| Modeling Process | Module | Specific Operations |
|---|---|---|
| Pre-processing | Part | Establishing models of Solid-Homogeneous in equal proportions, including mortise, tenon, and adhesive layer. |
| | Assembly | Import and adjust the position of each part according to the actual situation. |
| | Mesh | Dimensions of contact part: 1×1×1(mm); Dimensions of non-contact part: 4×4×4(mm); Element type: wood (C3D8R); adhesive (COH3D8). |
| | Property | Type: (1) Wood: Orthotropic with Elastic and plastic constitutive model; (2) Cohesive: Defined as Maxs Damage criterion. Orientation: Created different coordinate systems to assign the direction of two materials. |
| Load Solver | Interaction | Interaction: Defined the fit and friction coefficient of arc-part of connection. Constraint: Tied the contact surface between the adhesive layer and the joint up; Bound the mortise and tenon to different reference point. |
| | Load | Applied boundary conditions to constrain the uniaxial displacement of mortise and tenon. |
| | Step | Field output: stress and strain; History output: displacement and force of reference point. |
| | Job | Data check and calculation. |
| Post processing | Visualization | Stress-strain cloud map and force-displacement curve. |



**Fig. 5.** Finite element model of I-type mortise-and-tenon joint. (a) Finite element model of I-type joint; (b) Cohesive elements attached to tenon member

## Statistical Analysis

The effects of the fits between mortise and tenon of I-type joints on the tensile strength of evaluated specimens were analyzed by the analysis of variance (ANOVA) general linear model (GLM) procedure using SPSS (IBM, version 27, Armonk, USA) at the 5% significance level. A finite element model was established using the method described above to simulate the experimental tests to get the tensile capacity and compare with the experimental results verify the rationality of the modeling method. All of the data were subjected to regression analysis to generate fitting formulas and curves.

## RESULTS AND DISCUSSION

## Failure Mode and Statistical Analysis of Machining Testing

*Failure mode*

All tenons were pulled out of mortises completely. As shown in Fig. 6, there are three typical modes of failure, among which Fig. 6(a) indicates that neither mortise nor tenon suffered significant damage, and little wood fiber tearing could be observed on the surface. This indicated that the adhesive layer was mainly damaged at this time, and the bonding effect was not ideal. In Fig. 6(b), the tenon was damaged during extraction with a large amount of tenon tissue remaining in the mortise; conversely, in Fig. 6(c), the mortise was damaged, and a large number of mortise tissue was brought out when the tenon was pulled out. These two situations fully demonstrated that when the bonding interface was in close contact, the shear strength of the adhesive layer was much greater than the strength of the material itself. During this time, the joint underwent shear failure parallel-to-grain, and the bonding effect was better.
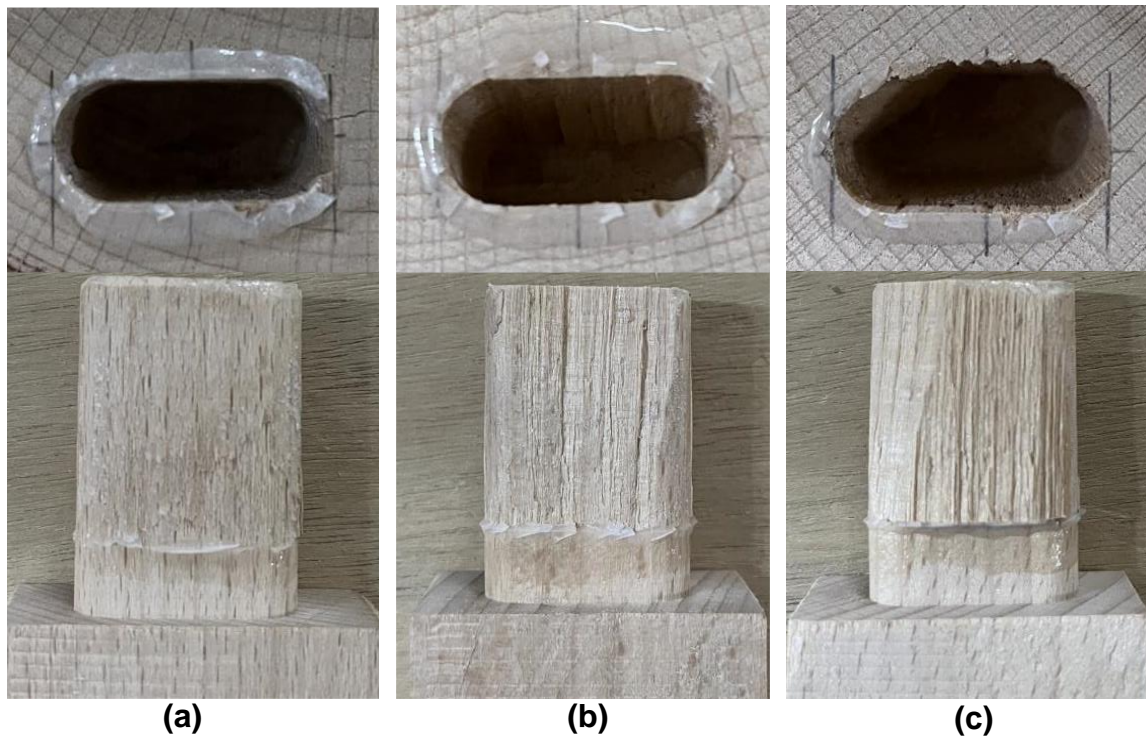


**(a)**                    **(b)**                    **(c)**

**Fig. 6.** Three types of failure mode of I-type mortise-and-tenon joint

At the same time, it can be observed that there was almost no tearing or damage of wood fibers in the width direction of the tenon, that is, the arc-part of the tenon, while all of this occurred in the flat-part of the tenon. Therefore, it can be inferred that although the same interference fit, there was a greater deformation in the width direction of the tenon, and almost all the adhesive was squeezed out. This phenomenon also verified the rationality of finite element modeling.

Wood failure ratio means the percentage of the total area of residual wood on the failure surface of the specimen to the shear area of the specimen. This study compared the difference of failure modes of joints under 5 fits from a macro perspective by observing and evaluating the wood failure ratio, as well as calculating the average value for each group.

As shown in Table 3, by estimating and calculating the wood failure ratio of each group of specimens, it can be concluded that the maximum values of tensile strength of each group occurred in the several specimens with the highest wood failure ratio. Comparing the average ratios between 5 groups, the higher average wood failure ratio indicated greater tensile strength.

**Table 3.** Estimation of Average Wood Failure Ratio of Different Fits

| Groups of Different Fit (mm) | Average Wood Failure Ratio |
|:---:|:---:|
| -0.3 | 40% |
| -0.2 | 55% |
| -0.1 | 68% |
| 0 | 76% |
| 0.1 | 80% |

Based on the above content, it can be inferred that the clearance fits between the mortise and tenon was too large to make the contact surface bonded tightly, so that there would not form an adhesive layer effectively. Therefore, the shearing strength of adhesive layer was much lower than the parallel shear strength of the wood itself, and the bonding state is not ideal. On the contrary, the interference fit made for a better adhesive layer to increase the bonding and tensile strength.

*Statistical analysis*

The statistical results of 5 groups of specimens are shown in Table 4, and a line chart with error bar is plotted as shown in Fig. 7(a). The average of maximum pull-out load rose with the increase of fit amount. When the interference fit was 0.1 mm, the average load reached its maximum value of 16000 N among 5 groups, which was 4110 N and 34.8% higher than the minimum average value of 11800 N when the clearance fit was -0.3 mm.

Meanwhile, the average value was about twice as much as the M&T joint when subjected to tensile load (Derikvand *et al.* 2014; Hu *et al*. 2020). This result is consistent with the conclusion that the shear strength of wood parallel to the grain is twice that of the perpendicular to the grain (Rakesh and Arijit 2012). So, shear failure of material resulted in the pull-out of joints.

**Table 4.** Estimation of Average Wood Failure Ratio of Different Fits

| Projects | Groups of Different Fits (mm) | | | | |
|---|---|---|---|---|---|
| | -0.3 | -0.2 | -0.1 | 0 | 0.1 |
| Maximum load (N) | 13479.70 | 17569.40 | 18748.40 | 20389.40 | 19195.00 |
| Minimum load (N) | 9821.90 | 12431.30 | 13070.30 | 10772.50 | 13716.30 |
| Average load (N) | 11836.93 | 14319.50 | 15046.48 | 15645.37 | 15978.66 |
| Standard deviation (N) | 1009.30 | 1251.96 | 1518.62 | 2165.36 | 1713.63 |
| Coefficient of variation | 8.53% | 8.74% | 10.09% | 10.96% | 9.20% |

The effect of fits on the tensile strength of I-type joints was analyzed by the ANOVA, the value of p was less than 0.001, indicating that the value of fits has a significant impact on the dependent variable. By conducting regression analysis on the results, a regression equation was obtained between the tensile load *y* (N) and the fit-ting amount a (mm) as shown in Eq. 1. The significance level p was less than 0.001, and the fitting degree $R^2$ was 0.9764, representing a high degree of fit. The fitting curve is shown in Fig. 7(a). It can be observed that the larger the fit value, the tighter the contact, and the higher the shear strength of the formed adhesive layer and tensile strength of the joint. When the fit is over -0.1 mm, the tensile load still increased, but the slope of the curve began to decrease, so the growth rate was significantly reduced.

$$y = -312.98x^2 + 2834.3x + 9512.5 \qquad (1)$$
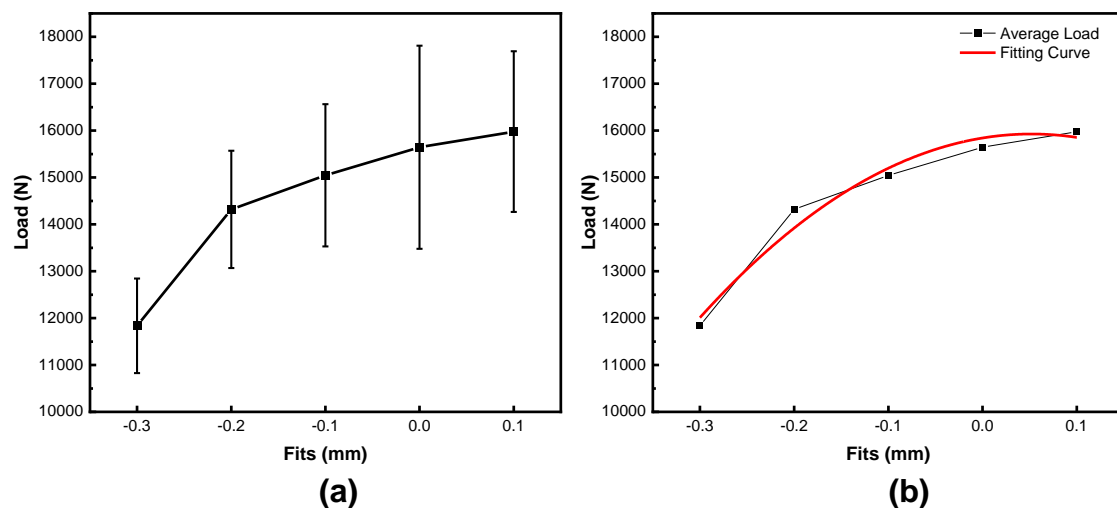


**Fig. 7.** Line chart (a) and fitting curve (b) of tensile strength of I-type joint

**Analysis of Finite Element Model**

When the interference fit was 0.1 mm, the stress cloud diagram was as shown in Fig. 8. The arc-part of the tenon was always compressed because of the interference fit during the tensile process, and the adhesive layer attached to the flat-part experienced shear damage was subject to failure ultimately.

To clarify the failure mode of joint, the stress cloud map of the tenon was separately examined, as shown in Fig. 9. When the tensile load started to be applied, the adhesive layer on the flat-part of the tenon produced a significant bonding strength to resist pull-out force. As the load continued to increase, the adhesive layer began to undergo shear failure

and the pull-out force decreased. However, due to the close contact between the tenon and mortise, there was still frictional force acting on the contact surface. The failure mode of FEM was similar to the mechanical test results.

## Comparative Analysis of Mechanical Experiment and FEM

*Comparison of tensile capacity*

Table 5 and Fig. 10(a) show results of comparison between the maximum pull-out load of finite element model and mechanical test. The maximum value of FEM was 14300 N, which was less than the average experimental value of 16000 N, with an error of 10.5%. This error may be due to the fact that the finite element modeling process did not simulate the actual situation of both interference fit and adhesive layer bonding at the joints. Rather, the FEM analysis only simulated interference fit in the arc-part and adhesive bonding in the plane surface.

**Table 5.** Results of Comparison Between the Maximum Tensile Load of Finite Element Model and Mechanical Test

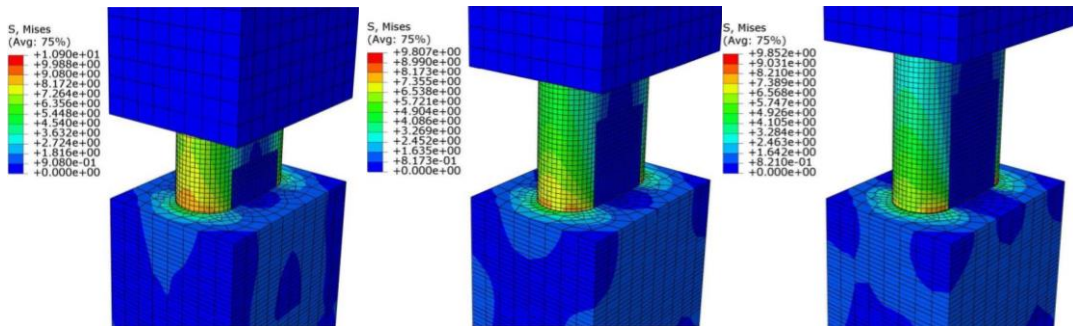| Results of Mechanical Testing (N) | | Result of FEM (N) | Error Value |
|---|---|---|---|
| Average load | 15978.66 | | |
| Maximum load | 19195.00 | 14304 | 10.48% |
| Minimum load | 13716.30 | | |



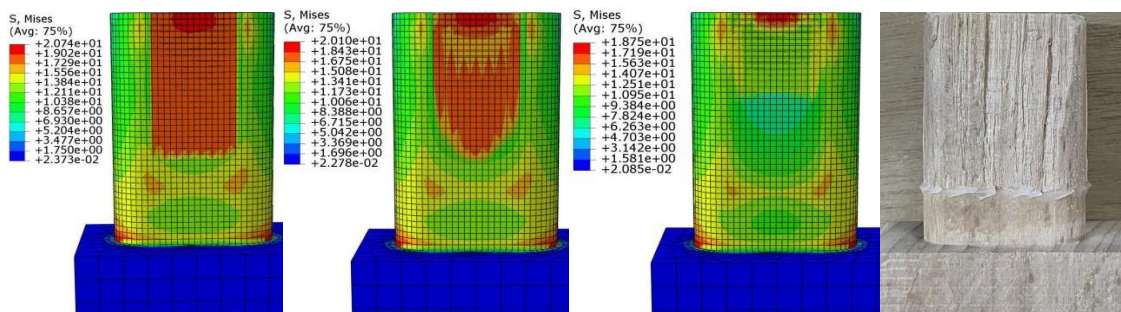**Fig. 8.** Stress distributions of I-type joint during withdrawal process



**Fig. 9.** Stress distributions of tenon member during withdrawal process when the interference fit is 0.1 mm

*Comparison of mechanical behavior*

The comparison of load displacement curve between the finite element analysis results and the mechanical tests under the same interference fit is shown in Fig. 10(b) The maximum tensile capacity obtained from the finite element model was between the

maximum and minimum values of the experimental results. In mechanical tests, the pull-out load dropped sharply after it reached its maximum value, and then the pull-out force fluctuated around 0 N continuously. Although the finite element simulation value rapidly decreased after reaching the maxi-mum pull-out force, the decrease rate was smaller than the experimental value; and then the tensile load continued to decline, as well as the rate of decrease, until the tenon was pulled out completely. This difference may be due to the pull-out of the tenons caused by the shear failure of adhesive layer and material in the test specimens was instantaneous, while the finite element model was defined as ductile damage.
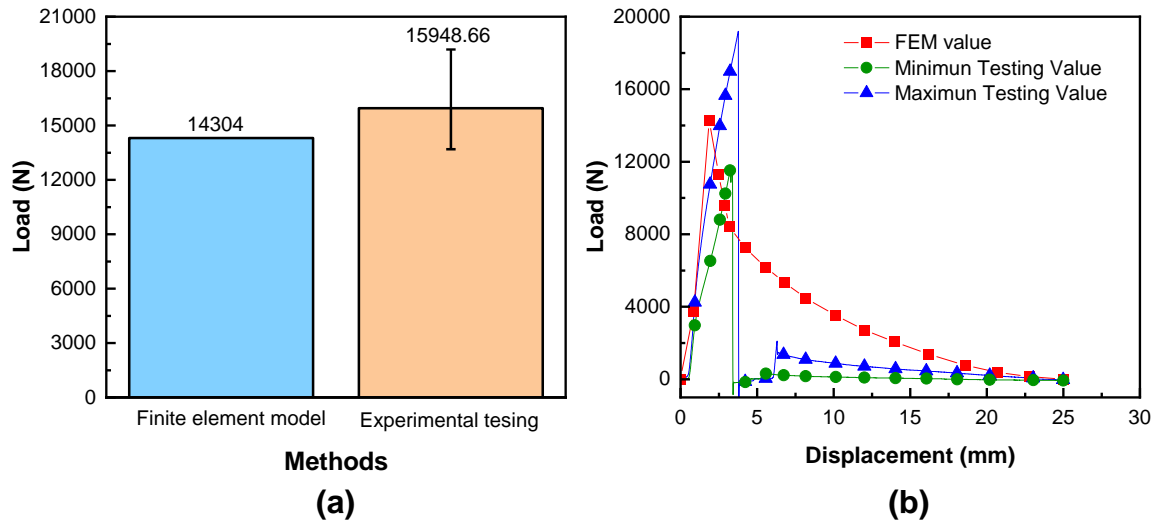


**Fig. 10.** (a) Histogram of comparison between the maximum simulated pull-out load of finite element model and the average of maximum load of mechanical test; (b) Comparison of load-displacement curve between FEM and mechanical experiments

Based on the above analysis, even though there is an error between the finite element model and mechanical test results, the error value was within an acceptable range. The data also verifies the rationality of the finite element model simulation.

## CONCLUSIONS

1. The value of fit had an important impact on the withdrawal capacity of I-type joint. The largest average pull-out load occurred at the group of 0.1 mm interference fit with the value of 16,000 N. The bonding strength was higher, so the joint underwent shear failure of material parallel-to-grain during the testing.

2. Finite element model is a rational approach to predict the withdrawal strength of parallel-to-grain connection part of M&LT joint. The maximum value of FEM was 14300 N, which was less than the average experimental value of 16000 N, with an error of 10.5%, which can be regarded as within an acceptable range.

3. This study provided a connection method for the diversification of furniture appearance design, and subsequent research can be expanded to multiple aspects such as bending moment capacity and torsion resistance capacity; or be delved into the microscopic perspective to observe the penetration of glue and the changes in wood cells.

## ACKNOWLEDGMENTS

## REFERENCES CITED

Bayatkashkoli, A., Ardakani, M. R., Hosseini-Tabatabaei, M. R., and Madahi, N. K. (2017). "Investigation of the maximum front to back load in the chairs made from curved and modified poplar wood," *Journal of Wood Science* 63(6), 580-590. DOI: 10.1007/s10086-017-1650-3

Chen, B., and Guan, H. (2023). "A novel method and validation for obtaining the optimal interference fit of round-end mortise-and-tenon joint," *Wood Material Science & Engineering* 18(5), 1619-1629. DOI:10.1080/17480272.2023.2165451

Derikvand, M., and Ebrahimi, G. (2014). "Strength performance of mortise and loose-tenon furniture joints under uniaxial bending moment," *Journal of Forestry Research* 25(2) 483-486. DOI: 10.1007/s11676-014-0479-5

Derikvand, M., Smardzewski, J., Ebrahimi, G., Dalvand, M., and Maleki, S. (2013). "Withdrawal force capacity of mortise and loose tenon T-type furniture joints," *Turkish Journal of Agriculture and Forestry* 37(3), 377-384. DOI:10.3906/tar-1204-8

Diler, H., Acar, M., Balikci, E., Demirci, S., and Erdil, Y. Z. (2017). "Withdrawal force capacity of T-Type furniture joints constructed from various heat-treated wood species," *BioResources* 12(4), 7466-7478. DOI: 10.15376/biores.12.4.7466-7478

Dong, C., Yang, Y., Zhang, H., Chui, Y. H., and Chen, T. (2017). "Modeling and experimental validation of elastic modulus of *Pinus yunnanensis* exposed to high relative humidity," *Wood Science and Technology* 51(5), 1015-1031. DOI: 10.1007/s00226-017-0923-8

Dzincic, I., and Skakic, D. (2012). "Influence of type of fit on strength and deformation of oval tenon-mortise joint," *Wood Research* 57(3), 469-477.

Fu, W. L., and Guan, H. Y. (2022). "Numerical and theoretical analysis of the contact force of oval mortise and tenon joints concerning outdoor wooden furniture structure," *Wood Science and Technology* 56(4), 1205-1237. DOI: 10.1007/s00226-022-01395-w

Fu, W., Guan, H., and Chen, B. (2021). "Investigation on the influence of moisture content and wood section on the frictional properties of beech wood surface," *Tribology Transactions* 64(5), 830-840. DOI: 10.1080/10402004.2021.1926029

Fu, W. L., Guan, H. Y., and Zhang, X. Y. (2020). "Verification and further study on method of measuring contact force between mortise and tenon joint," *BioResources* 16(1), 263-276. DOI: 10.15376/biores.16.1.263-276

Fu, W. L., Guan, H. Y. and Kei, S. (2021). "Effects of moisture content and grain direction on the elastic properties of beech wood based on experiment and finite element method," *Forests* 12(5), 610-626. DOI: 10.3390/f12050610

Gao, L. L., Xu, W., and Huang, Q. T. (2019). "Research on strength optimization of split elliptical tenon structure," *Furniture* 40(6), 24-29. DOI: 10.16610/j.cnki.jiaju.2019.06.006.

Hao, J., Xu, L., Wu, X., and Li, X. (2020). "Analysis and modeling of the dowel connection in wood T type joint for optimal performance," *Composite Structures* 253-

263. DOI: 10.1016/j.compstruct.2020.112754

Hu, W., and Chen, B. (2021). "A methodology for optimizing tenon geometry dimensions of mortise-and-tenon joint wood products," *Forests* 12(4), 478-489. DOI: 10.3390/f12040478

Hu, W., and Guan, H. (2019). "A finite element model of semi-rigid mortise-and-tenon joint considering glue line and friction coefficient," *Journal of Wood Science* 65(1), 14-22. DOI: 10.1186/s10086-019-1794-4

Hu, W., Liu, N., and Guan, H. (2019). "Experimental study of the contact forces and deformations of mortise-and-tenon joints considering the fits and grain orientations of the tenon," *BioResources* 14(4), 8728-8737.

Hu, W., Liu, N., and Guan, H. (2020). "Experimental and numerical study on methods of testing withdrawal resistance of mortise-and-tenon joint for wood products," *Forests* 11(3), 280-288. DOI: 10.3390/f11030280

Hu, W. G., and Guan, H. Y. (2018). "Study on contact force relaxation behavior of mortise-and-tenon joints considering tenon fits and grain orientations of tenon," *BioResources* 13(3), 5608-5616. DOI: 10.15376/biores.13.3.5608-5616

Imirzi, H. O., Smardzewski, J., and Dongel, N. (2015). "Method for substitute modulus determination of furniture frame construction joints," *Turkish Journal of Agriculture and Forestry* 39(5), 775-785. DOI: 10.3906/tar-1406-92

Jung, K., Hwang, K., and Komatsu, K. (2006a). "Effect of changes in the moisture content due to surrounding relative humidity on the contact stress in traditional mortise and tenon joints I. Effects of komisen insertion and joint drying on the contact stress between end grain of column and still," *Mokuzai Gakkaishi* 52(1), 44-49. DOI: 10.2488/jwrs.52.44

Jung, K., Hwang, K., and Komatsu, K. (2006b). "Effect of changes in the moisture content due to surrounding relative humidity on the contact stress in traditional mortise and tenon joints II. Evaluation of anti-relaxation effects by deformation recovery of compressed wooden Komisen on the contact stress of joints," *Mokuzai Gakkaishi* 52(3), 153-159. DOI: 10.2488/jwrs.52.153

Jung, K., Kitamori, A., Leijten, A. J. M., and Komatsu, K. (2006c). "Effect of changes in the moisture content due to surrounding relative humidity on the contact stress in traditional mortise and tenon joints III. Pull-out strength of compressed sugi komisen joints," *Mokuzai Gakkaishi* 52(6), 358-367. DOI: 10.2488/jwrs.52.358

Kasal, A., Haviarova, E., Efe, H., Eckelman, C. A., and Erdil, Y. Z. (2013). "Effect of adhesive type and tenon size on bending moment capacity and rigidity of T-shaped furniture joints constructed of Turkish beech and Scots pine," *Wood Fiber Sci.* 45(3), 287-293.

Lokaj, A., Dobes, P., and Sucharda, O. (2020). "Effects of loaded end distance and moisture content on the behavior of bolted connections in squared and round timber subjected to tension parallel to the grain," *Materials (Basel, Switzerland)* 13(23), article 5525. DOI: 10.3390/ma13235525

Miao, Y., Pan, S., and Xu, W. (2022). "Staple holding strength of furniture frame joints constructed of plywood and solid wood," *Forests* 13(12), 2006-2017. DOI: 10.3390/f13122006

Ogawa, K., Sasaki, Y., and Yamasaki, M. (2016). "Theoretical estimation of the mechanical performance of traditional mortise tenon joint involving a gap," *Journal of Wood Science* 62(3), 242-250. DOI: 10.1007/s10086-016-1544-9

Oktaee, J., Ebrahimi, G., Layeghi, M., Ghofrani, Eckelman, Carl, A. (2014). "Bending

---

moment capacity of simple and haunched mortise and tenon furniture joints under tension and compression loads," *Turkish Journal of Agriculture & Forestry* 38, 291-297. DOI: 10.3906/tar-1211-74

Rakesh, G., and Arijit, S. (2012). "Effect of grain angle on shear strength of Douglas-fir wood," *Holzforschung* 66(5), 655-658. DOI: 10.1515/hf-2011-0031

Ramon Villar-Garcia, J., Vidal-Lopez, P., Corbacho, A. J., and Moya, M. (2020). "Determination of the friction coefficients of chestnut (*Castanea sativa* Mill.) sawn timber," *International Agrophysics* 34(1), 65-77. DOI: 10.31545/intagr/112270

Ratnasingam, J., and Ioras, F. (2013). "Effect of adhesive type and glue-line thickness on the fatigue strength of mortise and tenon furniture joints," *European Journal of Wood and Wood Products* 71(6), 819-821. DOI: 10.1007/s00107-013-0724-1

SjöDin, J., Serrano, E., and Enquist, B. (2008). "An experimental and numerical study of the effect of friction in single dowel joints," *Holz als Roh und Werkstoff* 66(5), 363-372. DOI: 10.1007/s00107-008-0267-z

Smardzewski, J. (2002). "Strength of profile-adhesive joints," *Wood Science and Technology* 36(2), 173-183. DOI: 10.1007/s00226-001-0131-3

Vassilios, V., Ioannis B., and Vasiliki K. (2016). "Strength of corner and middle joints of upholstered furniture frames constructed with black locust and beech wood," *Wood Research* 61(3), 495-504.

Xie, Q., Zhang, B., Zhang, L., Guo, T., and Wu, Y. (2021). "Normal contact performance of mortise and tenon joint: theoretical analysis and numerical simulation," *Journal of Wood Science* 67(1), 31-51. DOI: 10.1186/s10086-021-01963-x

Xu, X., Xiong, X., Yue, X., and Zhang, M. (2023). "A parametric optimized method for three-dimensional corner joints in wooden furniture," *Forests* 14(5), 1063-1078. DOI: 10.3390/f14051063

Yue, X. Y., Xiong, X. Q., Xu, X. T., and Zhang, M. (2024). "Big data for furniture intelligent manufacturing: conceptual framework, technologies, applications, and challenges," *The International Journal of Advanced Manufacturing Technology* 132, 5231-5247. DOI: 10.1007/s00170-024-13719-0